CHEMISTRY OF MATERIALS

ARTICLE

pubs.acs.org/cm

Direct Attachment of Oligonucleotides to Quantum Dot Interfaces

Hyunjoo Han, Joshua Zylstra, and Mathew M. Maye*

Department of Chemistry, Syracuse University, Syracuse, New York 13244, United States

Supporting Information

ABSTRACT: A straightforward functionalization strategy for the direct attachment of single-stranded oligonucleotides (ssDNA) to quantum dot (qdot) interfaces is described. The approach takes advantage of a histidine-mediated phase transfer protocol that results in qdots with high colloidal stability in aqueous buffers. The weakly bound histidine encapsulation facilitates monolayer exchanged with both thiolated ssDNA and polyhistidine-tagged proteins. The successful biomodification at the qdot interface was probed by FRET analysis. The modest FRET efficiencies measured suggest the DNA to be in an extended conformation that is the result of high surface coverage that the direct attachment provides.

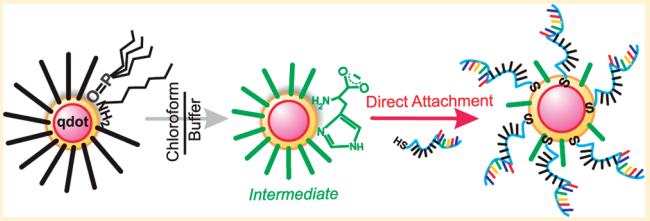

KEYWORDS: self-assembly, quantum dot, FRET, Qdot FRET, DNA, histidine

INTRODUCTION

The field of nanomaterial self-assembly has grown considerably recently and led to a number of exciting bottom-up morphologies, properties, and fundamental discoveries.[1−3] Strategies for nanomaterial self-assembly include the use of self-assembled monolayers,[4−6] polymers and dendrimers,[6−10] and multidentate ligands[11−15] to mediate recognition and cross-linking. Researchers have also focused on devising novel biomimetic assembly approaches,[16−20] where cross-linking interactions mimic biological recognition, or employ biological matter itself.[1−3,18−25] Examples include antibody−antigen[21,22] and DNA-based recognition.[23−25] The DNA-mediated assembly of nanomaterials, such as gold nanoparticles, has proven to be especially powerful in both a fundamental and application perspective.[23−34] In these systems, the nanoparticle interface is directly coated with thiol-modified oligonucleotides that form a dense surface capping layer.[26] This oligonucleotide brush passivates the interface, providing colloidal stability under physiological conditions.[23−26,34] When combined with a nanoparticle with bound complementary oligonucleotides, cross-linking occurs via hybridization and duplex DNA formation.[23,24] By varying sequence, structure, and coverage, important self-assembly parameters can be controlled; such as interparticle distances,[27] hydrodynamic diameters,[28] and kinetics,[28,29] as well as DNA denaturation temperatures.[30] In addition, it was recently shown that such parameter and interaction control can lead to the DNA-guided bulk crystallization of nanoparticles with long-range order, and lattice constants up to 100 nm.[31−33] The interparticle DNA-linkage also allows researchers to tailor interparticle distances by varying the number of linkage DNA sequences.[27,31,33] This has allowed fundamental studies on the distance-dependent optical responses and further colorimetric detection strategies,[34] such as plasmon ruler examples,[35−37] and fluorescence quenching based assays and studies.[38−40]

Recently, this research has broadened to devising new functionalization strategies for programming semiconductive quantum dots (qdots) with similar DNA-mediated reactivity.[40−45] Because these qdots have the added functionality of size-tunable photoluminescence,[46,47] assembled qdot structures have utility in biological sensing as well as bioimaging. However, unlike gold nanoparticles which are synthesized in aqueous conditions with large diameters (e.g., 10−50 nm), qdots are typically synthesized in nonpolar solvents via organometallic methods, and have much smaller sizes (e.g., 2−5 nm).[48−50] This introduces a number of challenges that must be overcome for DNA functionalization.[41−45] These include the necessity for both phase transfer and colloidal stability, followed by multistep oligonucleotide coupling.[41−45] Phase transfer has been achieved using a number of methods, such as polymer wrapping,[51−55] lipid coating,[56,57] and monolayer based methods.[58−60] Once transferred, oligonucleotides functionalization is achieved using classical carbodiimide (EDC) coupling chemistry,[61,62] polyhistidine peptide DNA assembly,[63] and biotin−avidin recognition.[21]

Once functionalized, the interface can be probed using the Förster (or fluorescence) resonance energy transfer (FRET) method, where the qdot is the fluorescent donor, and a fluorophore acceptor is attached in proximity by a DNA linkage. A number of DNA−qdot FRET studies have been performed.[63−67] For instance, a nanosensor based on FRET capable of detecting low concentrations of target DNA has been developed.[63] In addition, linear DNA templates labeled with a series of acceptor dyes have been hybridized with qdots, showing a series of consecutive FRET processes.[64,65] In these cases, the DNA was linked to the qdot surface by either a terminal biotin or an oligohistidine peptidyl sequence. Cyclodextrin-encapsulated qdots and G-Quadruplex functionalized qdots have also been fabricated using an initial glutathione surface encapsulation.[66,67] There have

Received: July 27, 2011
Revised: October 1, 2011
Published: October 20, 2011

also been examples of functionalization strategies that allow for the "direct" attachment of oligonucleotides to qdots.[68−71] In these studies, thiolated oligonucleotides were either bound via ligand exchange with mercaptopropionic acid encapsulation after phase transfer,[68,70] or introduced during ZnS shell growth.[71] One benefit of approaches like these is the reduced number of functionalization steps required, and the similarities to the gold nanoparticle approaches, thus simplifying the synthetic design.

In this paper we describe a new approach that allows for the direct attachment of oligonucleotides to the qdot interface without the requirement of additional coupling procedures. This method utilizes the small molecule L-histidine (His, ***2***) to induce qdot phase transfer from nonpolar solvents to aqueous buffers.[72] This His-intermediate encapsulation is easily exchanged with thiol-modified oligonucleotides, making the approach closely resemble those used for metal nanoparticles. A similar approach is also shown for polyhistidine-tagged proteins. The success of the oligonucleotide functionalization was probed by FRET analysis.

MATERIALS AND METHODS

Cadmium oxide (CdO, 99.99%), sulfur (S, 100 mesh), zinc acetate (ZnAc, 99.99%), trioctylphosphine oxide (TOPO, 90%), 1-octadecene (ODE, 90%), oleylamine (OAm, 90%), dodecylamine (DDA, 98%), tributylphosphine (TBP, 97%), boric acid (98%), sodium tetraborate (99.98%), sodium phosphate monobasic monohydrate ($NaH_2PO_4 \cdot H_2O$, 98.0−102.0%), sodium phosphate dibasic hepta-hydrate ($Na_2HPO_4 \cdot 7H_2O$, 98.0−102.0%), L-histidine (His, ***2*** > 99%), 6-carboxy-X-rhodamine (ROX), and solvents including hexane, acetone, chloroform, and methanol were purchased from Sigma Aldrich. Selenium (Se, 99.99%, 200 mesh) was purchased from Alfa Aesar. Agarose was obtained from Acros organics. Ultrapure water (18.2 MΩ) was provided from a Sartorius Stedim Arium 61316 reverse osmosis unit combined with an Arium 611DI polishing unit. The *N*-terminus hexahistidine-tagged Streptavidin (*Stv*) was purchased from ProSpec-Tany TechnoGene Ltd. (Rehovot, Israel). Biotin- or thiol-functionalized oligonucleotides were purchased from IDT Inc.

Synthesis and Functionalization. *Quantum Dot Synthesis.* The CdSe/ZnS qdots (***1***-qdots) were synthesized in-house following traditional methods with slight modification to ligand concentrations.[48−50,72] In a typical synthesis, 0.025 g of CdO was dissolved in 3.0 mL of OAc by heating at 230 °C under Ar. Next, 0.005 mol of DDA and 0.5 g of TOPO were dissolved in 5.0 mL of ODE and heated to 270 °C where the solution became optically clear. At 270 °C, 0.118 g of Se dissolved in 1.0 mL of TBP was injected inducing nucleation and growth. The growth was quenched after a few seconds by injecting 10 mL of ODE at room temperature. The resulting CdSe qdots were then purified free of excess ligands by multiple methanol extractions, and finally by precipitation in acetone.[48−50] The DDA/TOPO-capped CdSe qdots were dried under N_2 and resuspended in chloroform. To prepare CdSe/ZnS core/shell qdots, a known amount of CdSe core was redispersed in ODE after evaporating chloroform and heated to 200 °C under Ar. The sulfur precursor (200 mM S dissolved in ODE) and the zinc precursor (200 mM zinc acetate dissolved in OAm) were injected sequentially in order to tailor ZnS growth, allowing a minimum of 10 min between injections to allow for shell annealing. The final zinc injection was in excess to ensure a zinc monolayer on the outermost surface of the qdot. After the final injection, the qdots were annealed for an additional 30 min to ensure shell quality. The reaction mixture was allowed to cool to room temperature and cleaned in the same manner as the core. The TOPO/DDA-CdSe/ZnS qdots (***1***-qdots) were then redispersed and stored in dried chloroform before undergoing ligand exchange. Analysis of the ***1***-qdots via transmission electron microscopy yielded an average qdot diameter of 4.4 ± 0.6 nm.

Phase Transfer and Purification. The as-synthesized DDA/TOPO-capped CdSe/ZnS qdots (**1**-qdot) were made soluble in aqueous media using the recently reported histidine-mediated phase transfer method.[72] Briefly, a known amount of ***1***-qdot ([***1***-qdot] 1−5 μM) was vigorously mixed with a 3000 molar excess of histidine (***2***) in a 3:1 methanol−water with 0.2 M NaOH. The resulting ***2***-qdots were then purified of excess DDA and TOPO ligands by back extracting with multiple chloroform rinses.[51] The ***2***-qdots were purified free of excess ***2*** ligands by use of a molecular weight cutoff filter (100 kDa) and multiple rinsing with 10 mM borate buffer (pH = 8.3). The resulting ***2***-stabilized qdot had a 40% quantum yield and was stored in the dark until needed.

DNA Functionalization and Assembly. The phase transferred ***2***-qdots were then modified with 3′-C_3-thiol modified oligonucleotides of ***A***-type (***A*** = 5′-CAG TGT AGA GAA TTT TT-C_3H_6-SH-3′). The ***A*** were first reduced from disulfides using 100 mM dithiolthreitol (DTT).[33] The reduced ***A*** was purified via a sephadex column (G-25, Amersham Bioscience) and eluted with 10 mM phosphate buffer (pH = 7.0). The ***A*** was quantified using the sequence-specific extinction coefficient. Next, the reduced ***A*** was added to a solution of the ***2***-qdots at a molar ratio of [***A***]:[***2***-qdot] = 6−16, in which the [***2***-qdot] is typically between 5 and 7 μM in 10 mM borate buffer (pH = 8.3).

To prepare the *Stv*-functionalized qdots, the *Stv* expressed with a hexahistidine modified *N*-terminus was added at a molar ratio of [*Stv*]:[***2***-qdot] = 4, in which [***2***-qdot] is typically between 5 and 7 μM in 10 mM borate buffer (pH = 8.3). The *Stv* was stored as received (20 mM Tris-HCl, pH = 7.5, [*Stv*] = 59 μM). This *Stv*−qdot mixture was incubated for 2 h at 15 °C in the dark. Next, the *Stv*-qdot were incubated with 3′-biotinylated ***A***-type ssDNA (***A*** = 5′-CAG TGT AGA GAA TTT TT-Biotin-3′) at a 4× molar ratio to the bound *Stv* (i.e., [***2***-qdot]:[*Stv*]:[***A***] = 1:4:16). The final ***A***/*Stv*-qdot was further incubated for 2 h before purification as described above. An identical procedure was used to modify the *Stv*-qdots with the longer biotinylated A_2-type ssDNA sequence (A_2 = 5′-AGA CAG TGT AGA GAA $(TTT)_5$-Biotin-3′).

Hybridization with the fluorescently tagged ***A***′-type ssDNA (***A***′= 5′-TCT ACA CTG TCT TTT-ROX-3′) was achieved by hybridization with either ***A***-qdot or ***A***/*Stv*-qdot (A_2/*Stv*-qdot) by combining in buffer (10 mM borate buffer, 50 mM NaCl, pH = 8.3). Assembly occurs due to the ***A***/***A***′ recognition of 12 base-pairs (bp). The assembly, and subsequent FRET studies were performed at a series of dye/qdot (acceptor/donor) ratios *n*, (*n* = [***A***′-ROX]/[***A***-qdot] = 0−40). The qdot and dye acceptor concentration was determined spectrophotometrically. The assembly reactions were incubated for 1 h in the dark before FRET analysis. In the present systems all qdots were from the same synthesis and phase transfer batch to ensure comparability.

Instrumentation. *UV−visible Spectrophotometry (UV−vis).* The UV−vis measurements were collected on a Varian Cary100 Bio UV−vis spectrophotometer between 200 and 900 nm. The instrument is equipped with an 8-cell automated holder with high precision Peltier heating controller.

Photoluminescence (PL). The PL emission and excitation measurements were collected on a Fluoromax-4 photon counting

spectrofluorometer (Horiba Jobin Yvon). The instrument is equipped with a 150 W xenon white light excitation source and computer-controlled monochromator. The detector is a R928P high sensitivity photon counting detector that is calibrated to emission wavelength. All PL emission and excitation spectra were collected using both wavelength correction of source intensity and detector sensitivity. The excitation wavelength is 400 nm using 3 nm excitation and emission slits unless otherwise noted. The instrument is equipped with a computer-controlled temperature controller provided by a Thermo NESLAB temperature recirculator (Thermo Scientific).

Calculations. *Qdot Concentration.* The qdot concentrations were calculated based on UV−vis optical absorption measurements of the qdot first band edge absorption (1s-1s) intensity using qdot size dependent optical extinction coefficients (ε_{qdot}).[73−75] In this study, an ε_{qdot} value of 81 150 (±16 000) M^{-1} cm^{-1} was determined based on the first band edge absorption of 530 nm for the CdSe/ZnS qdot.

Quantum Yield. The qdot photoluminescence quantum yields (QY) were calculated based on comparison to a reference dye using standard methods (eq 1)[76]

$$QY_{qdot}(\%) = QY_R\left(\frac{Abs_R}{Abs_{qdot}}\right)\left(\frac{PL_{qdot}}{PL_R}\right)\left(\frac{\eta^2_{qdot}}{\eta^2_R}\right) \quad (1)$$

where QY_R is the reference dye quantum yield (rhodamine = 31%, rhodamine 6G = 95%), and Abs_R and Abs_{qdot} are the optical absorption at specific excitation for the reference dye and qdot samples, respectively. Here, careful attention was paid to prepare samples with optical absorption below 0.10 in order to limit inner filter effects. PL_R and PL_{qdot} correspond to the total area of the PL emission after wavelength dependent calibration of both the excitation source, and photoluminescence detector, as well as after PL spectra baseline correction.

Förster Resonance Energy Transfer (FRET) Calculations. In FRET, the Förster distance (R_0) is calculated using eq 2[46,47,77]

$$R_0^6 = 8.8 \times 10^{23} k_p^2 \eta_D^{-4} Q_D J \quad (2)$$

where η_D is refractive index of the medium (η_D = 1.0), k_p is the polarization parameter (k_p = 2/3), Q_D is the donor quantum yield (Q_D = 32%), and J is the spectral overlap integral. The J value can be calculated using eq 3

$$J = \int f_D(\lambda)\varepsilon_A(\lambda)\lambda^4 d\lambda \quad (3)$$

where λ is the defined wavelengths of the donor−acceptor spectral overlap (λ = 450 − 650 nm), $f_D(\lambda)$ is the integrated donor emission, and $\varepsilon_A(\lambda)$ represents the integrated acceptor absorption using the acceptor extinction coefficient (ε_A = 82 000 M^{-1} cm^{-1}). The values of R_0 = 61.0 Å, and $J = 2.78 \times 10^{-13}$ cm^3 M^{-1} were calculated using eqs 2 and 3 as well as the software PhotoChemCAD.

Using the R_0 values calculated above, the FRET efficiency, E, was calculated using eq 4[46,47]

$$E = 1 - \frac{F_{DA}}{F_D} = \frac{nR_0^6}{nR_0^6 + r^6} \quad (4)$$

where F_{DA} is donor fluorescence in the presence of acceptor, F_D is fluorescence of the donor without acceptor, and n is the ratio between [donor]/[acceptor]. This can be experimentally measured by monitoring changes in the donor to acceptor fluorescence intensities, or changes in the fluorescence lifetime of the fluorophores. In this study, FRET efficiency was obtained by steady-state fluorescence measurements. All steady state intensities were baseline corrected, and the E values were calculated under the estimate that $n = 5 \pm 1$.

RESULTS AND DISCUSSION

The general strategy employed for qdot phase transfer and DNA functionalization is illustrated in Scheme 1. First, CdSe/ZnS qdots were synthesized via standard organometallic methods with slight modification.[48−50,72] The as-synthesized qdots were capped with both trioctylphosphine oxide (TOPO) and dodecylamine (DDA) (***1***-qdot). To initiate phase transfer to buffers, we employed the recently developed histidine (***2***) mediated method.[72] In this method, ***2*** is added to a solution of ***1***-qdot at a molar ratio of [***2***]:[***1***-qdot] = 3000. Vortexing the biphasic mixture for 1−5 min yields a ***2***-qdot phase transferred into buffer (10 mM borate buffer, pH = 8.3) in only minutes without significant precipitation. The resulting ***2***-qdots show good colloidal stability over months, and are used without additional treatment. The ***2***-qdots are then quantified by measuring the first band edge absorption via UV−vis, and compared using the size-dependent extinction coefficients using the calibration method recently described.[73−75] The UV−vis absorption and PL emission spectra reveal no spectral changes when compared to the ***1***-qdots. A decrease in quantum yield (QY) of ∼25% was typically measured for the ***2***-qdots compared to the ***1***-qdot precursors. This QY loss was also influenced by core size, as well as ZnS-shell thickness and quality, thus batch to batch values varied slightly. In this study, the ***2***-qdot possessed a QY of 32% compared to 53% for the as-synthesized ***1***-qdot.

One advantage of this phase transfer route is that the ***2***-capping provides a modest binding to the qdot interface. The ***2*** molecules are bound to the qdot interface via a bidentate ***2***-to-Zn^{2+} coordination, and the ZnS-shell of the qdots were purposely terminated with Zn^{2+} during synthesis.[72] We recently showed that this ***2***-capping can further undergo ligand exchange with self-assembled monolayers (SAMs), as well as mixed monolayers.[72] We used this favorable exchange property to directly modify the ***2***-qdot interface with single-stranded oligonucleotides (ssDNA), as well as polyhistidine-tagged proteins (Scheme 1, step 2). For instance, 3′-thiolated ssDNA encoded with sequence of type-***A*** (***A*** = 5′-CAG TGT AGA GAA TTT TT-3′) was added to a solution of purified ***2***-qdots at molar ratio of [***A***]:[qdot] ≈ 16 in 10 mM borate buffer and allowed to incubate for 2 h at RT, followed by a 3 h gradual increase in ionic strength from 0 to 50 mM NaCl. During this time, the direct attachment of ***A*** to the qdot interface occurs, via the displacement of the weakly bound ***2*** by the C_3-thiol linkage. A similar procedure was followed for the functionalization of ***2***-qdots with histagged streptavidin (*Stv*). In this case, the hexahistine at the *N*-terminus of the *Stv* binds to the Zn^{2+} terminated CdSe/ZnS qdot interface by displacing the bound ***2*** molecules. Similar binding has been shown for DHLA modified qdots.[40−47,59] To a solution of purified ***2***-qdots, the histagged *Stv* is added at a molar ratio of [*Stv*]:[qdot] ≈ 4 in 10 mM borate buffer and left to incubate as described above. Next, the *Stv*-qdots were incubated with 3′-biotinylated ***A***-type ssDNA at a molar ratio of [***A***]:[*Stv*] ≈ 4, and allowed to incubate in buffer, resulting in ***A***/*Stv*-qdots. Both the ***A***-qdots and ***A***/*Stv*-qdots were then purified free of excess ***A*** via

dx.doi.org/10.1021/cm2021593 |*Chem. Mater.* 2011, 23, 4975–4981

Scheme 1. Idealized Schematic Illustrating the Qdot Functionalization Steps Used in This Study (The *1*-qdots are Phase-Transferred from Chloroform to Aqueous Buffers Using Histidine (*2*), Forming *2*-qdots Dispersed in Borate Buffer (step 1). Next, the *2*-qdots are Directly Functionalized Using Either Thiolated *A*-type ssDNA (step 2a), or First with Histagged Streptavidin (*Stv*) Followed by Biotinylated *A* (step 2b). The Assembly between the *A*-qdots and *A*/*Stv*-qdots is Probed via FRET with the ROX Labeled *A*′-type ssDNA. Assembly Occurs Due to the 12 bp *A*/*A*′ dsDNA Hybridization)

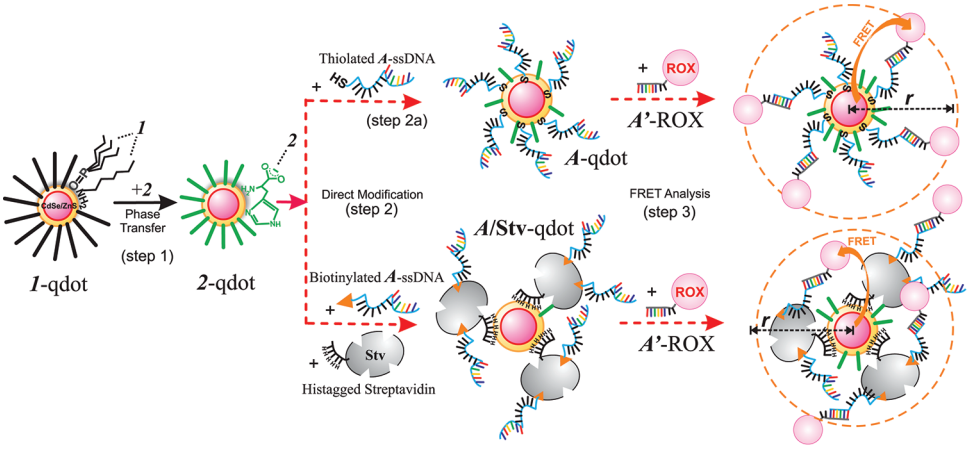

molecular weight (50 kDa) cutoff centrifugal filters, and quantified by UV−vis.

The direct functionalization of the *2*-qdots was first characterized via gel electrophoresis. Figure 1 shows a representative agarose gel result for the *2*-qdots before and after functionalization to *A*-qdot (a) and *A*/*Stv*-qdot (b) at increasing [*A*]:[*2*-qdot]. For instance, lanes 1 show the *2*-qdot (a) and *Stv*-qdot precursors (b) before *A*-modification. Interestingly, the *2*-qdots do not penetrate the gel due to precipitation in the running buffer.[72] However, upon attachment with thiolated *A*, the improved mobility of *A*-qdot in the gel is apparent by the mobility of the sharp band, as shown in lanes 2−5. The modest increase in mobility with [*A*]:[*2*-qdot] up to 40 (lanes 2−5) suggests an increase in coverage. Similar results were obtained for the *Stv*-qdots after modification with biotinylated-*A*. The *Stv*-qdots have minimal initial mobility due to similar instability and decrease in surface charge (Figure 1b), and the improved mobility of the initial *A*/*Stv*-qdots at [*A*]:[*2*-qdot] up to 40. Interestingly, the mobility remains similar despite increases in [*A*] (lanes 2−5). This suggests *A*-binding only to the accessible *Stv* recognition sites and not the qdot interface.

These gel results are strong qualitative evidence for direct ssDNA modification of the qdot interface. It is interesting to note that this modification procedure follows functionalization strategies similar to protocols found for DNA modification of citrate-capped gold nanoparticles,[23−34] and is in contrast to conventional approaches to modify qdots with ssDNA.[41−45] It is important to note that a few other direct attachment strategies have also been shown.[68−71] For instance, Mirkin and co-workers used mercaptopropionic acid (MPA) to modify qdots, followed by monolayer exchange with thiolated ssDNA.[68] A similar MPA-based method was also shown,[70] as well as approaches which bind ssDNA during ZnS shell growth.[71] Our approach is similar, but is not limited or hindered by the thiol−thiol monolayer exchange. A key question however is the nature of the ssDNA at the qdot interface, its coverage, structure, and accessibility.

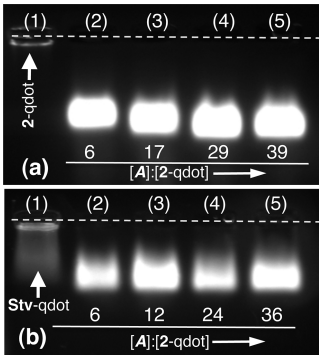

Figure 1. (a) Agarose gel results characterizing the *2*-qdots before (1) and after thiolated *A*-type ssDNA functionalization to *A*-qdots (2−5) at increasing [*A*]:[*2*-qdot] = 6−39 (1.0% agarose, 1× TBE, 70 V, 30 min). (b) Results for the *Stv*-qdots before (1) and after biotinylated *A*-type ssDNA functionalization to *A*/*Stv*-qdots (2−5) at increasing *r* = 6−36 (0.8% agarose, 1× TBE, 25 V, 60 min). Images collected under UV excitation.

We investigated this using FRET between the DNA-qdots and complementary ssDNA modified with a fluorophore. A number of reports have used FRET to better understand biofunctionalized qdot interfaces.[38−45] The qdot/dye FRET pair is analogous to classical FRET pairs, and the qdot itself has been well modeled as a single point dipole, due to the nature of the single exciton generation localized at the CdSe core.[47] This FRET system consists of the *A*-qdots and *A*/*Stv*-qdots prepared above with PL emission at 550 nm acting as FRET donors (D), whereas a complementary ssDNA of *A*′-type modified with a fluorescent dye (ROX) with emission at 605 nm serving as the FRET acceptor (A). The fluorophore ROX was chosen to sufficiently separate donor−acceptor emission spectra, while maintaining an acceptable overlap integral. The spectral properties and FRET efficiency plot are shown in Figure 2.

dx.doi.org/10.1021/cm2021593 |*Chem. Mater.* 2011, 23, 4975–4981

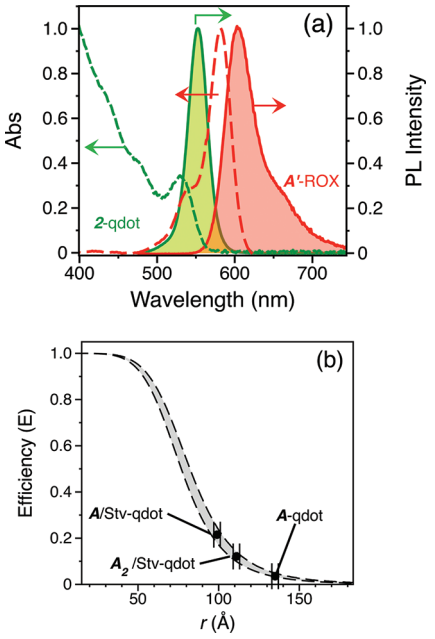

Figure 2. (a) Normalized PL emission and absorption spectra for 550 nm emitting **2**-qdot donor and ***A***′-ROX acceptor. (b) FRET efficiency curve calculated using eq 4 at R_0 = 61.0 Å and n = 4, 5, and 6. Inserted experimental E results for the labeled assembly systems.

A typical FRET profile between the ***A***-qdot and ***A***′-ROX at acceptor/donor ratios (n = [***A***′-ROX]/[***A***-qdot]) of 0−40 is shown in Figure 3a. A FRET efficiency (E) based on the quenching of the ***A***-qdot emission was calculated to be 3%. From analysis of the gel results (Figure 1, Figures S1 and S2), we approximate that each ***A***-qdot contains 5 (±1) ***A***-type ssDNA molecules. With this maximum number of potential ***A***′-ROX binding sites available, we calculated the FRET efficiency plot using eq 5 at n = 4−6, as shown in Figure 2b. From this plot, along with the measured E = 3%, we estimate the qdot-to-ROX distance (r, center-to-center), of $r \approx$ 14.2 (±0.4) nm. This is larger than an ideal estimate of ∼10 nm. This estimate is based on the number of base-pairs in the dsDNA linkages (12bp) and the length of the unlinked poly-T base segments in a coiled state (5b and 3b),[33] as well as the radius of the qdot (2.2 nm) and the radius of the ROX molecule (∼1 nm). The $r \approx$ 14 nm suggests a high coverage of ***A*** at the qdot interface, which leads to large amounts of interchain steric effects of the ssDNA polymer brush, thus extending the bound recognition sequences (3′-end) further from the qdot interface.

We next investigated the ***A***/*Stv*-qdot system for FRET with ***A***′-ROX. Figure 3b shows a typical FRET response at n = 0−40. Compared to the previously discussed ***A***-qdot system, an increased FRET efficiency of $E \approx$ 21% is measured. The ***A***/*Stv*-qdot was prepared at ratios in which a maximum of 5 (±1) ***A***-type ssDNA molecules were bound, in order for comparison. As shown in the FRET efficiency plots (Figure 2b), an E value of this magnitude correlates to a $r \approx$ 10.0 (±0.4) nm. Interestingly, this value is slightly less than the ideal estimate of ∼12 nm, considering the increase as the result of the size of the *Stv* macromolecule (∼2 nm). We further probed the ***A***/*Stv*-qdot systems by using an analogue ssDNA sequence to ***A***-type that contained an increased number of bases (30b), A_2-type. The A_2/*Stv*-qdot was prepared via the methods described above, again with a

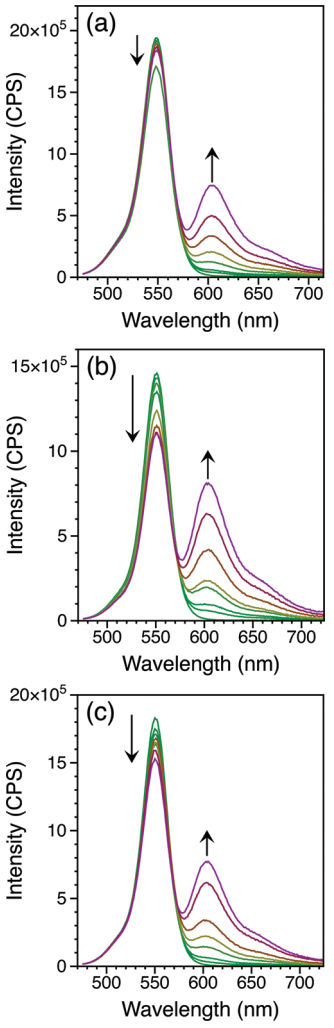

Figure 3. Representative emission spectra during a typical FRET experiment between ***A***-qdot (a), ***A***/*Stv*-qdot (b), and A_2/*Stv*-qdot (c) donors with ***A***′-ROX at $n \approx$ 2, 4, 7, 12, 21, 31, 42 (10 mM borate buffer, pH = 8.3, 50 mM NaCl, [qdot] = 10.1 nM, λ_{Ex} = 400 nm).

coverage of 5 (±1) A_2 molecules/qdot. A typical FRET spectra is shown in Figure 3c. As one might expect from the longer ssDNA sequence, a lower $E \approx$ 12% was calculated, which correlates with an $r \approx$ 11.1 (±0.4) nm. This value is also less than the ideal estimate of ∼13 nm that takes into account the additional 15b poly-T spacer segments.[27,28,33,77]

These results are representative of two trends consistently observed in our direct attachment studies. First, the thiol-modified ssDNA shows the lowest FRET efficiency, despite its seemingly shortest ideal distance. This demonstrates that the ***A***-qdot is sufficiently functionalized to the qdot in such a manner as to provide maximum coverage, and in turn to extend the recognition sequences residing at the terminus of the bound ssDNA, far from the qdot interface. In contrast, the ***A***/*Stv*-qdots have higher FRET efficiency and r-values lower than estimates. This can be understood by considering that the initial *Stv* layer will extend the attachment point of the ssDNA by ∼2 nm. Since the number of ssDNA/qdot is maintained, this results in sufficient free space near the qdot interface for approach, resulting in, on average, increased FRET efficiency. Using the longer ssDNA A_2/*Stv*-qdot analogue that showed decreased

dx.doi.org/10.1021/cm2021593 |*Chem. Mater.* 2011, 23, 4975–4981

efficiency substantiated this. Other factors may also play a role in the FRET efficiencies measured, such as a distribution of ZnS-shell thicknesses among the qdots used, as well the possibility of a distribution of ssDNA coverage across a qdot population. These factors, and further structural characterization, will be addressed in future work. Taken together, these results demonstrate that the direct attachment of ssDNA to a qdot interface does not necessarily result in optimum FRET. Other factors, such as surface coverage and surface accessibility are at play and also need to be engineered. Nevertheless, the histidine-mediated phase transfer method does provide a suitable qdot interface for the direct functionalization with oligonucleotides and his-tagged proteins, opening up a new route for the integration of qdots into increasingly sophisticated self-assembly designs.

CONCLUSION

These results demonstrate that the histidine-mediated phase transfer protocol provides an interface that is suitable for exchange with thiolated ssDNA, and histagged-proteins. Structural analysis via FRET indicates that the DNA−qdot interface binds with efficiency values at the high end of estimates that are based on DNA and protein structure alone. The observation that the thiolated ssDNA show the lowest FRET efficiency suggests a dense coverage of ssDNA that results in the unhybridized spacer regions conforming to a more extended state. In contrast the ssDNA bound to the initial streptavidin layer shows higher FRET efficiency due to the decreased sterics made possible by the low packing of the initial streptavidin layer, allowing for a more close approach by the ssDNA to the interface.

ASSOCIATED CONTENT

Supporting Information. Additional graphics. This material is available free of charge via the Internet at http://pubs.acs.org.

AUTHOR INFORMATION

Corresponding Author
*E-mail: mmmaye@syr.edu.

ACKNOWLEDGMENT

A Department of Defense PECASE award, sponsored by AFOSR (FA9550-10-1-0033), supported this work. We thank the Department of Chemistry and the Syracuse Biomaterials Institute (SBI) for start-up support.

REFERENCES

(1) Katz, E.; Willner, I. *Angew. Chem.* **2004**, *43*, 6042–6108.
(2) Zhang, Z. L.; Horsch, M. A.; Lamm, M. H.; Glotzer, S. C. *Nano Lett.* **2003**, *3*, 1341–1346.
(3) Daniel, M. C.; Astruc, D. *Chem. Rev.* **2004**, *104*, 293–346.
(4) (a) Templeton, A. C.; Wuelfing, W. P.; Murray, R. W. *Acc. Chem. Res.* **2000**, *33*, 27–36. (b) Devries, G. A.; Brunnbauer, M.; Hu, Y.; Jackson, A. M.; Long, B.; Neltner, B. T.; Uzun, O.; Wunsch, B. H.; Stellacci, F. *Science* **2007**, *315*, 358–361.
(5) (a) Freeman, R. G.; Grabar, K. C.; Allison, K. J.; Bright, R. M.; Davis, J. A.; Guthrie, A. P.; Hommer, M. B.; Jackson, M. A.; Smith, P. C.; Walter, D. G.; Natan, M. J. *Science* **1995**, *267*, 1629–1632. (b) Brust, M.; Kiely, C. J.; Bethell, D.; Schiffrin, D. J. *J. Am. Chem. Soc.* **1998**, *120*, 12367–12368.
(6) (a) Zheng, W.; Maye, M. M.; Leibowitz, F. L.; Zhong, C. J. *Anal. Chem.* **2000**, *72*, 2190–2199. (b) Zamborini, F. P.; Hicks, J. F.; Murray, R. W. *J. Am. Chem. Soc.* **2000**, *122*, 4514–4515.
(7) Frankamp, B. L.; Boal, A. K.; Rotello, V. M. *J. Am. Chem. Soc.* **2002**, *124*, 15146–15147.
(8) Boal, A. K.; Ilhan, F.; DeRouchey, J. E.; Thurn-Albrecht, T.; Russell, T. P.; Rotello, V. M. *Nature* **2000**, *404*, 746–748.
(9) Boal, A. K.; Rotello, V. M. *J. Am. Chem. Soc.* **2000**, *122*, 734–735.
(10) Carroll, J. B.; Frankamp, B. L.; Srivastava, S.; Rotello, V. M. *J. Mater. Chem.* **2004**, *14*, 690–694.
(11) (a) Lim, S. I.; Zhong, C. J. *Acc. Chem. Res.* **2009**, *42*, 798–808. (b) Lim, I. I. S.; An, D. L.; Vaiana, C.; Zhang, Z. Y.; Zhang, Y. J.; Zhong, C. J. *J. Am. Chem. Soc.* **2007**, *129*, 5368–5369.
(12) Maye, M. M.; Freimuth, P.; Gang, O. *Small* **2008**, *4*, 1941–1944.
(13) Lim, I. I.; Zhou, S. Q.; S.; Pan, Y.; Mott, D.; Ouyang, J.; Njoki, P. N.; Luo, J.; Zhong, C. J. *Langmuir* **2007**, *23*, 10715–10724.
(14) (a) Maye, M. M.; Lim, I. I. S.; Luo, J.; Rab, Z.; Rabinovich, D.; Liu, T.; Zhong, C. J. *J. Am. Chem. Soc.* **2005**, *127*, 1519–1529. (b) Maye, M. M.; Luo, J.; Lim, I. I. S.; Han, L.; Kariuki, N. N.; Rabinovich, D.; Liu, T.; Zhong, C. J. *J. Am. Chem. Soc.* **2003**, *125*, 9906–9907. (c) Maye, M. M.; Chun, S. C.; Han, L.; Rabinovich, D.; Zhong, C. J. *J. Am. Chem. Soc.* **2002**, *124*, 4958–4959.
(15) (a) Kairdolf, B. A.; Nie, S. *J. Am. Chem. Soc.* **2011**, *133*, 7268–7271. (b) Algar, W. R.; Krull, U. J. *Langmuir* **2006**, *22*, 11346–11352.
(16) Penn, S. G.; He, L.; Natan, M. J. *Curr. Opin. Chem. Biol.* **2003**, *7*, 609–615.
(17) Alivisatos, A. P. *Nat. Biotechnol.* **2004**, *22*, 47–52.
(18) (a) Quach, A. D.; Crivat, G.; Tarr, M. A.; Rosenzweig, Z. *J. Am. Chem. Soc.* **2011**, *133*, 2028–2030. (b) Shi, L.; De Paoli, V.; Rosenzweig, N.; Rosenzweig, Z. *J. Am. Chem. Soc.* **2006**, *128*, 10378–10379.
(19) (a) Slocik, J. M.; Tam, F.; Halas, N. J.; Naik, R. R. *Nano Lett.* **2007**, *7*, 1054–1058. (b) Heinz, H.; Farmer, B. L.; Pandey, R. B.; Slocik, J. M.; Patnaik, S. S.; Pachter, R.; Naik, R. R. *J. Am. Chem. Soc.* **2009**, *131*, 9704–9714. (c) Coppage, R.; Slocik, J. M.; Briggs, B. D.; Frenkel, A. I.; Heinz, H.; Naik, R. R.; Knecht, M. R. *J. Am. Chem. Soc.* **2011**, *133*, 12346–12349.
(20) (a) Zhang, C. Y.; Johnson, L. W. *J. Am. Chem. Soc.* **2006**, *128*, 5324–5325. (b) Zhang, C. Y.; Johnson, L. W. *Anal. Chem.* **2006**, *78*, 5532–5537.
(21) (a) Oh, E.; Hong, M. Y.; Lee, D.; Nam, S. H.; Yoon, H. C.; Kim, H. S. *J. Am. Chem. Soc.* **2005**, *127*, 3270–3271. (b) Cobbe, S.; Connolly, S.; Ryan, D.; Nagle, L.; Eritja, R.; Fitzmaurice, D. *J. Phys. Chem. B* **2003**, *107*, 470–477.
(22) Maye, M. M.; Freimuth, P.; Gang, O. *Small* **2008**, *4*, 1941–1944.
(23) Mirkin, C. A.; Letsinger, R. L.; Mucic, R. C.; Storhoff, J. J. *Nature* **1996**, *382*, 607–609.
(24) Alivisatos, A. P.; Johnsson, K. P.; Peng, X.; Wilson, T. E.; Loweth, C. J.; Bruchez, M. P., Jr.; Schultz, P. G. *Nature* **1996**, *382*, 609–611.
(25) Claridge, S. A.; Liang, H. W.; Basu, S. R.; Frechet, J. M.; Alivisatos, A. P. *Nano Lett.* **2008**, *8*, 1202–1206.
(26) (a) Lytton-Jean, A. K.; Mirkin, C. A. *J. Am. Chem. Soc.* **2005**, *127*, 12754–12755. (b) Demers, L. M.; Mirkin, C. A.; Mucic, R. C.; Reynolds, R. A.; Letsinger, R. L.; Elghanian, R.; Viswanadham, G. *Anal. Chem.* **2000**, *72*, 5535–5541. (c) Hurst, S. J.; Lytton-Jean, A. K.; Mirkin, C. A. *Anal. Chem.* **2006**, *78*, 8313–8318.
(27) Hill, H. D.; Macfarlane, R. J.; Senesi, A. J.; Lee, B.; Park, S. Y.; Mirkin, C. A. *Nano Lett.* **2008**, *8*, 2341–2344.
(28) (a) Maye, M. M.; Nykypanchuk, D.; van der Lelie, D.; Gang, O. *J. Am. Chem. Soc.* **2006**, *128*, 14020–14021. (b) Maye, M. M.; Nykypanchuk, D.; van der Lelie, D.; Gang, O. *Small* **2007**, *3*, 1678–1682.
(29) Prigodich, A. E.; Lee, O. S.; Daniel, W. L.; Seferos, D. S.; Schatz, G. C.; Mirkin, C. A. *J. Am. Chem. Soc.* **2010**, *132*, 10638–10641.
(30) Jin, R.; Wu, G.; Li, Z.; Mirkin, C. A.; Schatz, G. C. *J. Am. Chem. Soc.* **2003**, *125*, 1643–1654.

(31) Nykypanchuk, D.; Maye, M. M.; van der Lelie, D.; Gang, O. *Nature* **2008**, *451*, 549–552.
(32) Park, S. Y.; Lytton-Jean, A. K.; Lee, B.; Weigand, S.; Schatz, G. C.; Mirkin, C. A. *Nature* **2008**, *451*, 553–556.
(33) (a) Maye, M. M.; Kumara, M. T.; Nykypanchuk, D.; Sherman, W. B.; Gang, O. *Nat. Nanotechnol.* **2010**, *5*, 116–120. (b) Maye, M. M.; Nykypanchuk, D.; Cuisinier, M.; van der Lelie, D.; Gang, O. *Nat. Mater.* **2009**, *8*, 388–391.
(34) Rosi, N. L.; Mirkin, C. A. *Chem. Rev.* **2005**, *105*, 1547–1562.
(35) Liu, G. L.; Yin, Y.; Kunchakarra, S.; Mukherjee, B.; Gerion, D.; Jett, S. D.; Bear, D. G.; Gray, J. W.; Alivisatos, A. P.; Lee, L. P.; Chen, F. F. *Nat. Nanotechnol.* **2006**, *1*, 47–52.
(36) Sonnichsen, C.; Reinhard, B. M.; Liphardt, J.; Alivisatos, A. P. *Nat. Biotechnol.* **2005**, *23*, 741–745.
(37) Jain, P. K.; El-Sayed, M. A. *Nano Lett.* **2007**, *7*, 2854–2858.
(38) Gueroui, Z.; Libchaber, A. *Phys. Rev. Lett.* **2004**, *93*, 166108–166111.
(39) (a) Singh, M. P.; Strouse, G. F. *J. Am. Chem. Soc.* **2010**, *132*, 9383–9391. (b) Jennings, T. L.; Singh, M. P.; Strouse, G. F. *J. Am. Chem. Soc.* **2006**, *128*, 5462–5467. (c) Yun, C. S.; Javier, A.; Jennings, T.; Fisher, M.; Hira, S.; Peterson, S.; Hopkins, B.; Reich, N. O.; Strouse, G. F. *J. Am. Chem. Soc.* **2005**, *127*, 3115–3119.
(40) Pons, T.; Medintz, I. L.; Sapsford, K. E.; Higashiya, S.; Grimes, A. F.; English, D. S.; Mattoussi, H. *Nano Lett.* **2007**, *7*, 3157–3164.
(41) Algar, W. R.; Krull, U. J. *Langmuir* **2008**, *24*, 5514–5520.
(42) Gill, R.; Willner, I.; Shweky, I.; Banin, U. *J. Phys. Chem. B* **2005**, *109*, 23715–23719.
(43) Zhang, B.; Zhang, Y.; Mallapragada, S. K.; Clapp, A. R. *ACS Nano* **2011**, *5*, 129–138.
(44) Lu, H.; Schops, O.; Woggon, U.; Niemeyer, C. M. *J. Am. Chem. Soc.* **2008**, *130*, 4815–4827.
(45) Robelek, R.; Niu, L.; Schmid, E. L.; Knoll, W. *Anal. Chem.* **2004**, *76*, 6160–6165.
(46) (a) Clapp, A. R.; Medintz, I. L.; Mattoussi, H. *Phys. Chem. Chem. Phys.* **2006**, *7*, 47–57. (b) Delehanty, J. B.; Mattoussi, H.; Medintz, I. L. *Anal. Bional. Chem.* **2009**, *393*, 1091–1105.
(47) Medintz, I. L.; Mattoussi, H. *Phys. Chem. Chem. Phys.* **2009**, *11*, 17–45.
(48) Qu, L.; Peng, X. *J. Am. Chem. Soc.* **2002**, *124*, 2049–2055.
(49) Talapin, D. V.; Mekis, I.; Gotzinger, S.; Kornowski, A.; Benson, O.; Weller, H. *J. Phys. Chem. B* **2004**, *108*, 18826–18831.
(50) Li, J. J.; Wang, Y. A.; Guo, W.; Keay, J. C.; Mishima, T. D.; Johnson, M. B.; Peng, X. *J. Am. Chem. Soc.* **2003**, *125*, 12567–12575.
(51) (a) Lees, E. E.; Nguyen, T. L.; Clayton, A. H. A.; Muir, B. W.; Mulvaney, P. *ACS Nano* **2009**, *3*, 1121–1128. (b) Lees, E. E.; Gunzburg, M. J.; Nguyen, T. L.; Howlett, G. J.; Rothacker, J.; Nice, E. C.; Clayton, A. H. A.; Mulvaney, P. *Nano Lett.* **2008**, *8*, 2883–2890.
(52) Smith, A. M.; Duan, H.; Rhyner, M. N.; Ruan, G.; Nie, S. *Phys. Chem. Chem. Phys.* **2006**, *8*, 3895–3903.
(53) Dahan, M.; Levi, S.; Luccardini, C.; Rostaing, P.; Riveau, B.; Triller, A. *Science* **2003**, *302*, 442–445.
(54) Liu, W.; Howarth, M.; Greytak, A. B.; Zheng, Y.; Nocera, D. G.; Ting, A. Y.; Bawendi, M. G. *J. Am. Chem. Soc.* **2008**, *130*, 1274–1284.
(55) Pellegrino, T.; Manna, L.; Kudera, S.; Liedl, T.; Koktysh, D.; Rogach, A. L.; Keller, S.; Radler, J.; Natile, G.; Parak, W. J. *Nano Lett.* **2004**, *4*, 703–707.
(56) Yu, W. W.; Chang, E.; Falkner, J. C.; Zhang, J. Y.; Al-Somali, A. M.; Sayes, C. M.; Johns, J.; Drezek, R.; Colvin, V. L. *J. Am. Chem. Soc.* **2007**, *129*, 2871–2879.
(57) Mulder, W. J. M.; Skajaa, T.; Zhao, Y. M.; van den Heuvel, D. J.; Gerritsen, H. C.; Cormode, D. P.; Koole, R.; van Schooneveld, M. M.; Post, J. A.; Fisher, E. A.; Fayad, Z. A.; Donega, C. D.; Meijerink, A. *Nano Lett.* **2010**, *10*, 5131–5138.
(58) Dubertret, B.; Skourides, P.; Norris, D. J.; Noireaux, V.; Brivanlou, A. H.; Libchaber, A. *Science* **2002**, *298*, 1759–1762.
(59) (a) Mattoussi, H.; Mauro, J. M.; Goldman, E. R.; Anderson, G. P.; Sundar, V. C.; Mikulec, F. V.; Bawendi, M. G. *J. Am. Chem. Soc.* **2000**, *122*, 12142–12150. (b) Jaiswal, J. K.; Mattoussi, H.; Mauro, J. M.; Simon, S. M. *Nat. Biotechnol.* **2003**, *21*, 47–51. (c) Medintz, I. L.; Uyeda, H. T.; Goldman, E. R.; Mattoussi, H. *Nat. Mater.* **2005**, *4*, 435–446.
(60) (a) Cohen, B. E.; Han, G.; Mokari, T.; Ajo-Franklin, C. *J. Am. Chem. Soc.* **2008**, *130*, 15811–15813. (b) Gao, J. H.; Chen, K.; Xie, R. G.; Xie, J.; Lee, S.; Cheng, Z.; Peng, X. G.; Chen, X. Y. *Small* **2010**, *6*, 256–261. (c) Yang, M.; Tsang, E. M.; Wang, Y. A.; Peng, X.; Yu, H. Z. *Langmuir* **2005**, *21*, 1858–1865.
(61) Dhar, S.; Daniel, W. L.; Giljohann, D. A.; Mirkin, C. A.; Lippard, S. J. *J. Am. Chem. Soc.* **2009**, *131*, 14652–14653.
(62) Zhou, D.; Ying, L.; Hong, X.; Hall, E. A.; Abell, C.; Klenerman, D. *Langmuir* **2008**, *24*, 1659–1664.
(63) Zhang, C. Y.; Yeh, H. C.; Kuroki, M. T.; Wang, T. H. *Nat. Mater.* **2005**, *4*, 826–831.
(64) Boeneman, K.; Deschamps, J. R.; Buckhout-White, S.; Prasuhn, D. E.; Blanco-Canosa, J. B.; Dawson, P. E.; Stewart, M. H.; Susumu, K.; Goldman, E. R.; Ancona, M.; Medintz, I. L. *ACS Nano* **2010**, *4*, 7253–7266.
(65) Boeneman, K.; Prasuhn, D. E.; Blanco-Canosa, J. B.; Dawson, P. E.; Melinger, J. S.; Ancona, M.; Stewart, M. H.; Susumu, K.; Huston, A.; Medintz, I. L. *J. Am. Chem. Soc.* **2010**, *132*, 18177–18190.
(66) Freeman, R.; Finder, T.; Gill, R.; Willner, I. *Nano Lett.* **2010**, *10*, 2192–2196.
(67) Sharon, E.; Freeman, R.; Willner, I. *Anal. Chem.* **2010**, *82*, 7073–7077.
(68) Mitchell, G. P.; Mirkin, C. A.; Letsinger, R. L. *J. Am. Chem. Soc.* **1999**, *121*, 8122–8123.
(69) Mahtab, R.; Harden, H. H.; Murphy, C. J. *J. Am. Chem. Soc.* **2000**, *122*, 14–17. (b) Mahtab, R.; Rogers, J. P.; Murphy, C. J. *J. Am. Chem. Soc.* **1995**, *117*, 9099–9100.
(70) Zhou, D.; Piper, J. D.; Abell, C.; Klenerman, D.; Kang, D. J.; Ying, L. *Chem. Commun.* **2005**, 4807–4809.
(71) Wang, Q.; Liu, Y.; Ke, Y.; Yan, H. *Angew. Chem.* **2008**, *47*, 316–319.
(72) Zylstra, J.; Amey, J.; Miska, N. J.; Pang, L.; Hine, C. R.; Langer, J.; Doyle, R. P.; Maye, M. M. *Langmuir* **2011**, *27*, 4371–4379.
(73) Yu, W. W.; Qu, L.; Guo, W.; Peng, X. *Chem. Mater.* **2003**, *15*, 2854–2860.
(74) Liu, Y.; Kim, M.; Wang, Y.; Wang, Y. A.; Peng, X. *Langmuir* **2006**, *22*, 6341–6345.
(75) Jasieniak, J.; Smith, L.; van Embden, J.; Califano, M.; Mulvaney, P. *J. Phys. Chem. C.* **2009**, *113*, 19468–19474.
(76) Lakowicz, J.R. *Principles of Fluorescence Spectroscopy*, 2nd ed.; Kluwer Academic/Plenum Publishers: New York, 1999.
(77) Brenner, H. *Int. J. Multiphase Flow* **1974**, *1*, 195–341.